Factors driving the seasonal and hourly variability of sea-spray aerosol number in the North Atlantic

Georges Saliba[a], Chia-Li Chen[a], Savannah Lewis[a], Lynn M. Russell[a,1], Laura-Helena Rivellini[b], Alex K. Y. Lee[b,c], Patricia K. Quinn[d], Timothy S. Bates[e], Nils Haëntjens[f], Emmanuel S. Boss[f], Lee Karp-Boss[f], Nicholas Baetge[g], Craig A. Carlson[g], and Michael J. Behrenfeld[h]

[a]Scripps Institution of Oceanography, University of California San Diego, La Jolla, CA 92093; [b]Environmental Research Institute, National University of Singapore, 117411, Singapore; [c]Department of Civil and Environmental Engineering, National University of Singapore, 117576, Singapore; [d]Pacific Marine Environmental Laboratory, National Oceanic and Atmospheric Administration, Seattle, WA 98115; [e]Joint Institute for the Study of the Atmosphere and Ocean, University of Washington, Seattle, WA 98195; [f]School of Marine Sciences, University of Maine, Orono, ME 04469; [g]Department of Ecology, Evolution, and Marine Biology, University of California, Santa Barbara, CA 93106; and [h]Department of Botany and Plant Pathology, Oregon State University, Corvallis, OR 97331

Edited by John H. Seinfeld, California Institute of Technology, Pasadena, CA, and approved August 21, 2019 (received for review May 4, 2019)

Four North Atlantic Aerosol and Marine Ecosystems Study (NAAMES) field campaigns from winter 2015 through spring 2018 sampled an extensive set of oceanographic and atmospheric parameters during the annual phytoplankton bloom cycle. This unique dataset provides four seasons of open-ocean observations of wind speed, sea surface temperature (SST), seawater particle attenuation at 660 nm ($c_{p,660}$, a measure of ocean particulate organic carbon), bacterial production rates, and sea-spray aerosol size distributions and number concentrations (N_{SSA}). The NAAMES measurements show moderate to strong correlations ($0.56 < R < 0.70$) between N_{SSA} and local wind speeds in the marine boundary layer on hourly timescales, but this relationship weakens in the campaign averages that represent each season, in part because of the reduction in range of wind speed by multiday averaging. N_{SSA} correlates weakly with seawater $c_{p,660}$ ($R = 0.36$, $P << 0.01$), but the correlation with $c_{p,660}$, is improved ($R = 0.51$, $P < 0.05$) for periods of low wind speeds. In addition, NAAMES measurements provide observational dependence of SSA mode diameter (d_m) on SST, with d_m increasing to larger sizes at higher SST ($R = 0.60$, $P << 0.01$) on hourly timescales. These results imply that climate models using bimodal SSA parameterizations to wind speed rather than a single SSA mode that varies with SST may overestimate SSA number concentrations (hence cloud condensation nuclei) by a factor of 4 to 7 and may underestimate SSA scattering (hence direct radiative effects) by a factor of 2 to 5, in addition to overpredicting variability in SSA scattering from wind speed by a factor of 5.

NAAMES | sea spray aerosol | phytoplankton bloom | radiative impacts

Sea-spray aerosol (SSA) particles are the largest source of natural aerosols to Earth's atmosphere on a mass basis (1). SSA particles affect climate directly by interacting with incoming solar radiation (2–4), as well as indirectly by acting as cloud condensation nuclei (CCN) that, in turn, impact cloud lifetime and precipitation patterns (5). The relative contribution of SSA to total aerosol load is greatest in the cleanest regions of the globe (oceans), making the climate response particularly sensitive to their concentrations (6–8). However, there are large uncertainties associated with the magnitude of SSA emission and removal fluxes, with published measurements and parameterizations of SSA number flux spanning over an order of magnitude in range (1, 9–11) (*SI Appendix*, Table S1).

SSA particles are produced through the action of wind stress on ocean surfaces and so a positive correlation exists between SSA mass and wind speed (12–15). Several SSA parameterizations used in global climate models are based largely on laboratory experiments (16–18) and are then scaled to field observations to better represent their range and variability across diverse atmospheric and ocean conditions (16, 19, 20). Changes in sea surface temperatures (SST), salinity, and surface-active agents alter water surface tension, density, and viscosity, which together influence bubble bursting mechanisms and rise time of bubbles to the surface (1, 11, 13, 16, 20–25). However, the quantitative relationship between these surface water properties and SSA formation and size differs significantly between published studies (1, 9, 11, 16, 23, 26, 27), highlighting the extent to which the mechanisms are still poorly understood.

There are a few SSA parameterizations that account for the influence of SST on SSA production (11, 21, 28, 29), and most of these parameterizations lack information on SSA size. Furthermore, few laboratory-based studies have investigated the effects of water-dissolved organic materials on SSA production (25, 30, 31), despite organic materials being highly concentrated at the ocean surfaces, particularly during phytoplankton blooms (32, 33). Failing to account for SSA production and size changes associated with varying ocean conditions (e.g., SST and seawater organic carbon) may bias modeled SSA concentrations for the marine boundary layer.

Significance

Sea-spray aerosol (SSA) particles are the largest source of natural aerosol to the atmosphere on a mass basis and contribute significantly to the direct and indirect radiative effects over oceans. The role of wind speed in driving SSA production is well known; however, the degree to which SSA production is influenced by other parameters, such as sea-surface temperature (SST) and seawater (phytoplankton derived) particulate organic carbon, remain poorly understood. Here, shipborne measurements spanning the full annual cycle of the North Atlantic phytoplankton bloom provide direct measurements of the influence of SST and ocean biomass on SSA number concentrations and diameter. Our results have significant implications for understanding SSA production and their radiative impacts in the marine boundary layer.

Author contributions: L.M.R., P.K.Q., T.S.B., C.A.C., and M.J.B. designed research; G.S., C.-L.C., S.L., L.-H.R., A.K.Y.L., N.H., E.S.B., L.K.-B., and N.B. performed research; G.S. and L.M.R. contributed new reagents/analytic tools; G.S., C.-L.C., P.K.Q., T.S.B., N.H., E.S.B., L.K.-B., N.B., and C.A.C. analyzed data; and G.S. and L.M.R. wrote the paper.

The authors declare no conflict of interest.

This article is a PNAS Direct Submission.

Data deposition: NAAMES atmospheric and ocean measurements are archived at https://www-air.larc.nasa.gov/missions/naames/index.html. Scripps measurements are available at https://library.ucsd.edu/dc/collection/bb34508432. Shipboard measurements are archived at https://seabass.gsfc.nasa.gov/.

[1]To whom correspondence may be addressed. Email: lmrussell@ucsd.edu.

This article contains supporting information online at www.pnas.org/lookup/suppl/doi:10.1073/pnas.1907574116/-/DCSupplemental.

We acknowledge that SSA emitted to the marine boundary layer will be affected by photochemistry, transport, and mixing such that direct correlations between seawater properties and the aerosol in the overlying atmosphere are tenuous. Correlations between properties also do not imply causation. However, the four NAAMES field campaigns enable an unprecedented evaluation of the seasonal dependence of SSA concentrations and diameter on wind speed, SST, and seawater particle attenuation at 660 nm ($c_{p,660}$, a measure of particulate organic carbon, POC; ref. 34). These observations allow improvements in field-based parameterizations of SSA formation that are necessary to better predict SSA concentrations (N_{SSA}) in the marine boundary layer and, ultimately, their radiative impact on Earth's climate.

Results and Discussion

The four seasons encompassed by NAAMES allow us to investigate both seasonal and hourly variability for clean marine conditions in both N_{SSA} and the mode diameter of the SSA number size distribution (d_m), which was obtained by fitting the 0.6 to 5.0 μm range of the measured size distribution with a single lognormal mode that, on average, has a full width at half maximum of 0.2 to 2.0 μm (*Methods* and *SI Appendix*, Text S2–S9). Real-time measurements of N_{SSA}, d_m, local wind speed at 18 m above sea level (U_{18}), $c_{p,660}$ (a measure of POC), bacterial production rates, and SST (*SI Appendix*, Fig. S1 and Table S2) show significant variability within each season. The larger variability in N_{SSA} compared to local wind speed within each campaign suggests that local wind speed alone cannot fully explain the observed variability in N_{SSA} (*SI Appendix*, Table S2). In contrast, d_m exhibits a more constrained range in variability (21 to 40%) that is similar to the variability in SST (14 to 42%), as shown in *SI Appendix*, Table S2.

Frequency histograms for d_m and the geometric SD (GSD) of the SSA number size distributions for all NAAMES campaigns (Fig. 1) show that the ranges spanned by d_m and GSD are large (0.05 to 1.1 μm for d_m and 1.5 to 4.0 for GSD). The differences in the 4 campaign average d_m values were statistically significant ($P << 0.01$ on ANOVA test). The retrieved d_m varies from a low of 0.42 ± 0.17 μm for late spring (NAAMES 2) to a high of 0.77 ± 0.20 μm for early spring (NAAMES 4), with this strong dependence of d_m with season giving the largest particles during the highest SST (Fig. 2 *B* and *D*).

The range in GSD observed during NAAMES (1.5 to 4.0; median = 2.1) is notably larger than the laboratory-constrained range of 2.5 to 3.0 reported by Modini et al. (35) and the field-based range of 2.2 to 2.8 reported by Quinn et al. (36). Similarly, the range for retrieved d_m (0.05 to 1.10 μm dry diameter) is significantly larger than those in published literature, which have typically placed the peak of the d_m at 0.1 to 0.3 μm dry diameter (1, 19, 35–37). However, significant variability in the size and width of the SSA size distribution has been observed under several ocean conditions (14, 22, 36, 37). The larger SSA sizes reported here are not explained by missing smaller SSA particles since accumulation-mode mass and chloride mass concentrations were not correlated (except weakly during NAAMES 3; *SI Appendix*, Fig. S2 and Text S8) and adding smaller SSA particles did not improve correlations with local wind speed (*SI Appendix*,

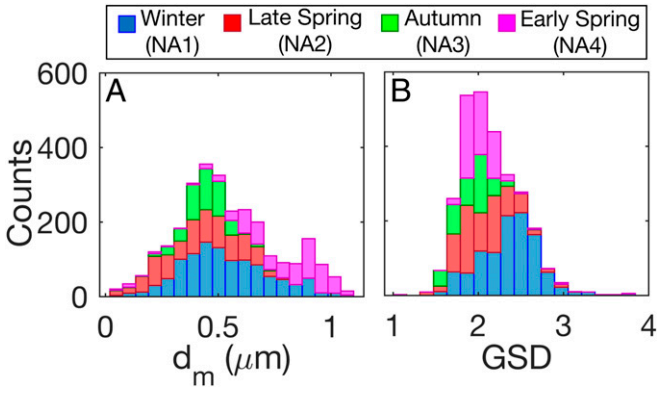

Fig. 1. Stacked frequency histograms for all NAAMES campaigns for (*A*) retrieved SSA mode diameter (d_m) and (*B*) retrieved SSA geometric SD (GSD).

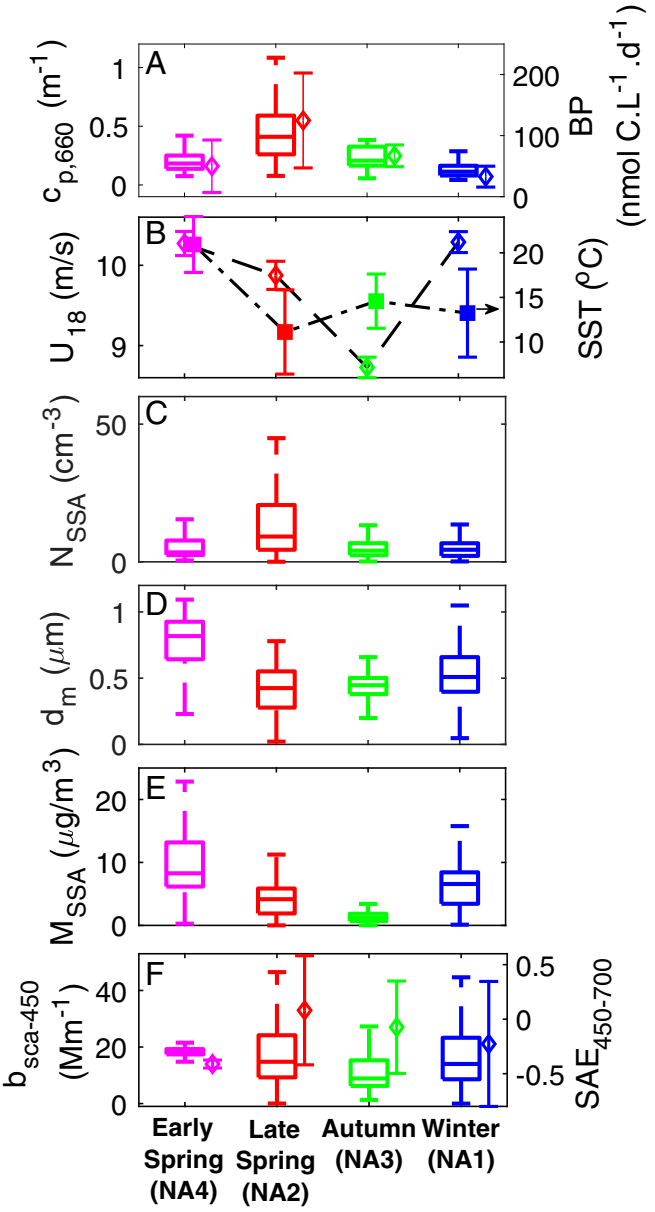

Fig. 2. Seasonal variability for (*A*) seawater particle attenuation at 660 nm ($c_{p,660}$) (boxplot, left *y* axis) and mixed-layer-integrated and depth-normalized bacterial production rates (BP, diamonds, right *y* axis), (*B*) mean local wind speed (U_{18}, open diamonds, left *y* axis) and average SST (filled squares, right *y* axis). The points in *B* are connected to guide the eye. (*C*) N_{SSA}, (*D*) SSA mode diameter (d_m), (*E*) M_{SSA} (assuming a spherical particles and unit density), and (*F*) scattering coefficient measured at 450 nm ($b_{sca-450}$ boxplots, left *y* axis) and scattering angstrom exponent calculated between 450 and 700 nm ($SAE_{450-700}$, right *y* axis). Boxes are interquartile range and horizontal lines are the medians. Error bars are the SD except for wind speed for which we show the SE ($SE = \sigma/\sqrt{N}$). Whiskers extend to ~90% (±2.7σ) of the data. Measurements are colored by campaign.

Text S5). NAAMES 4 started 15° farther south than the other campaigns, resulting in a larger range of latitudes as well as of retrieved N_{SSA}, d_m, and GSD. Nevertheless, the same trends are evident even if measurements south of 30°N are excluded (*SI Appendix*, Figs. S3 and S4).

Seasonal Variability. N_{SSA} during late spring (NAAMES 2) was 3 times higher than during winter (NAAMES 1) and early spring (NAAMES 4) despite lower mean wind speeds (U_{18}) measured during NAAMES 2 (*SI Appendix*, Fig. S2 and Table S2). The higher N_{SSA} in late spring could be due to a contribution from SSA particles that may have a higher organic fraction (and less sea salt) than typical for SSA particles. This is supported by the higher $c_{p,660}$ (a measure of POC) as well as higher bacterial production rates measured during NAAMES 2 (Fig. 2), since the latter suggests enriched bioavailable dissolved organic carbon (DOC) concentrations in the surface microlayer. However, N_{SSA} did not correlate with DOC concentrations sampled in the upper 10 m (*SI Appendix*, Fig. S5), which may be because the small dynamic fraction of the bulk DOC is obfuscated by the large (refractory) DOC that constitutes the majority of bulk DOC (38). The higher N_{SSA} in late spring could also be due to other factors such as transport from productive coastal regions, precipitation effects on particle scavenging, whitecaps extent and bubble production, and differences in boundary layer mixing.

NAAMES measurements do show a strong and significant correlation between median d_m and median SST on seasonal timescales ($R = 0.99$, $P < 0.05$; *SI Appendix*, Fig. S6). This finding is supported by a strong negative correlation observed between the median scattering angstrom exponent (SAE, which is inversely proportional to particle size) and median SST on seasonal timescales ($R = -0.98$, $P < 0.05$; *SI Appendix*, Fig. S6). These findings represent observational evidence for a link between SST and d_m on seasonal timescales and support the hypothesis that SSA diameter is affected by the changes in film drainage time and bubble retention time prior to bursting due to alteration of physical seawater properties (i.e., viscosity and surface tension) (31, 39). Atmospheric chemical reactions could also increase SSA mode diameter, but photochemistry is expected to be more active in late spring than in early spring.

Correlations of median N_{SSA} and SSA mass concentrations with median local wind speeds were not significant for seasonal averages (*SI Appendix*, Fig. S6). The lack of seasonal dependence on wind speed may be due to the small dynamic range in seasonal winds, since the relative standard deviation (RSD) of 4 seasonally averaged local wind speeds was only 8.1%.

Hourly Variability. The variability in hourly local wind speed during each campaign was much larger than the 8.1% seasonal variability, with RSD values for wind speed on hourly timescales ranging from 32 to 48% (*SI Appendix*, Table S2). The larger variability of local wind speeds within each campaign provides data to assess the dependence of N_{SSA} on wind speed in the marine boundary layer.

N_{SSA} was moderately correlated with local wind speed ($R = 0.5$, $P << 0.01$) during all NAAMES (Fig. 3*D*), with N_{SSA} increasing from less than 5 cm^{-3} at low wind speeds ($U_{18} < 5$ m s^{-1}) to more than 30 cm^{-3} at high wind speeds ($U_{18} > 20$ m s^{-1}). These values for N_{SSA} fall within the range of published data from field observations (13, 14, 22, 35, 36).

The fact that N_{SSA} did not always track local coincident wind speed is not surprising since parameters such as upwind wind speed, precipitation, sea state, marine boundary layer mixing, atmospheric photochemistry, and SST also influence SSA number concentrations (1). However, the moderate correlation does show that wind speed explains 25% of the observed variability. An additional 6 to 25% of the observed variability between N_{SSA} and wind speed is explained by seasonal differences, with Pearson's R improved from 0.50 (for all NAAMES) to 0.56 to 0.70 for individual campaigns (*SI Appendix*, Fig. S7). Separating the N_{SSA} versus wind speed measurements by campaign also reveals a lower increase in N_{SSA} with wind speeds for NAAMES 1 and 4 (with power law exponent below 1.5) compared to NAAMES 2 and 3 (with power law exponent above 1.9) (*SI Appendix*, Fig. S7). This observation provides further support that properties other than local wind speed significantly influence N_{SSA}.

The N_{SSA} parameterization from O'Dowd et al. (14) gives concentrations that are generally higher than the NAAMES N_{SSA} for wind speeds larger than 4 m s^{-1} (Fig. 3*D* and *SI Appendix*, Fig. S8), in agreement with a previous study (12). There is no evidence that this discrepancy could be explained by a separate SSA mode in the accumulation size range (*SI Appendix*, Text S5), which may have important implications for climate models because several studies (9, 21, 40) have used the Gong (18) SSA production function optimized to the O'Dowd et al. (14) results. These models, therefore, use SSA number concentrations (hence CCN) that are likely higher than those measured in the western subarctic Atlantic.

SST and surfactants have been shown to influence SSA production both in the laboratory and in the field (16, 20, 22–26), but even the sign of the dependence of N_{SSA} on SST and surfactants remains uncertain (1, 11). At hourly timescales, NAAMES N_{SSA} are weakly correlated ($R = 0.36$, $P << 0.01$) to $c_{p,660}$ (a measure of POC) for 15-min measurements for NAAMES (Fig. 3*E*). The strength of this correlation between N_{SSA} and $c_{p,660}$ is increased ($R = 0.51$, $P << 0.01$) when measurements are limited to conditions of low wind speeds, although the data remain heteroskedastic (*SI Appendix*, Fig. S9). However, the link from POC concentrations to N_{SSA} is not expected since some POC components are too large to contribute to N_{SSA}. For POC to explain some N_{SSA} variability, we speculate that the POC correlation to N_{SSA} could mean that as POC is processed through foodweb processes that some fraction is transformed to a colloidal or dissolved form. Estimated heterotrophic bacterial production could provide a proxy for this production of submicron colloidal DOC, since bacteria can only take up low-molecular-weight organic compounds. The strong positive correlation between $c_{p,660}$ (a measure of POC) and bacterial production rates ($R = 0.81$, $P << 0.01$; *SI Appendix*, Fig. S5) provides initial support for this hypothesis, but the heteroskedastic distribution relating bacterial production rates to N_{SSA} indicates that other mechanisms should also be considered ($R = 0.56$, $P < 0.05$; *SI Appendix*, Text S10 and Fig. S5). Regardless of the processes that contribute organic carbon to bubbles and the microlayer (33, 41), both the additional labile DOC and possibly also smaller POC could form particles together with sea salt and also separately (42), potentially explaining the increased SSA number.

N_{SSA} was not correlated with SST ($R = -0.2$; Fig. 3*F*) although SSA mass concentrations were weakly correlated with SST ($R = 0.30$, $P < <0.01$; *SI Appendix*, Fig. S10), consistent with laboratory and field observations (11, 21, 28, 29). In addition, d_m increased linearly with SST (Fig. 3*C*) from 0.38 ± 0.17 μm for 0 °C < SST < 5 °C to 0.77 ± 0.19 μm for 20 °C < SST < 25 °C ($R = 0.60$, $P << 0.01$). The correlation of the 4-campaign dataset is equal to or higher than that of the 4 separate campaigns (Pearson's R were 0.4 for NA1, 0.2 for NA2 and NA3, and 0.6 for NA4), consistent with the expectation that the larger dynamic range of SST in the 4-campaign dataset would provide a stronger correlation. Based on these results, we developed a new expression for the impacts of SST on d_m (Fig. 3*C*):

$$d_m = 2.3 \times 10^{-2} SST + 0.2,$$

which is a parameterization that could be introduced into future climate models. The measured increase in d_m with increased SST

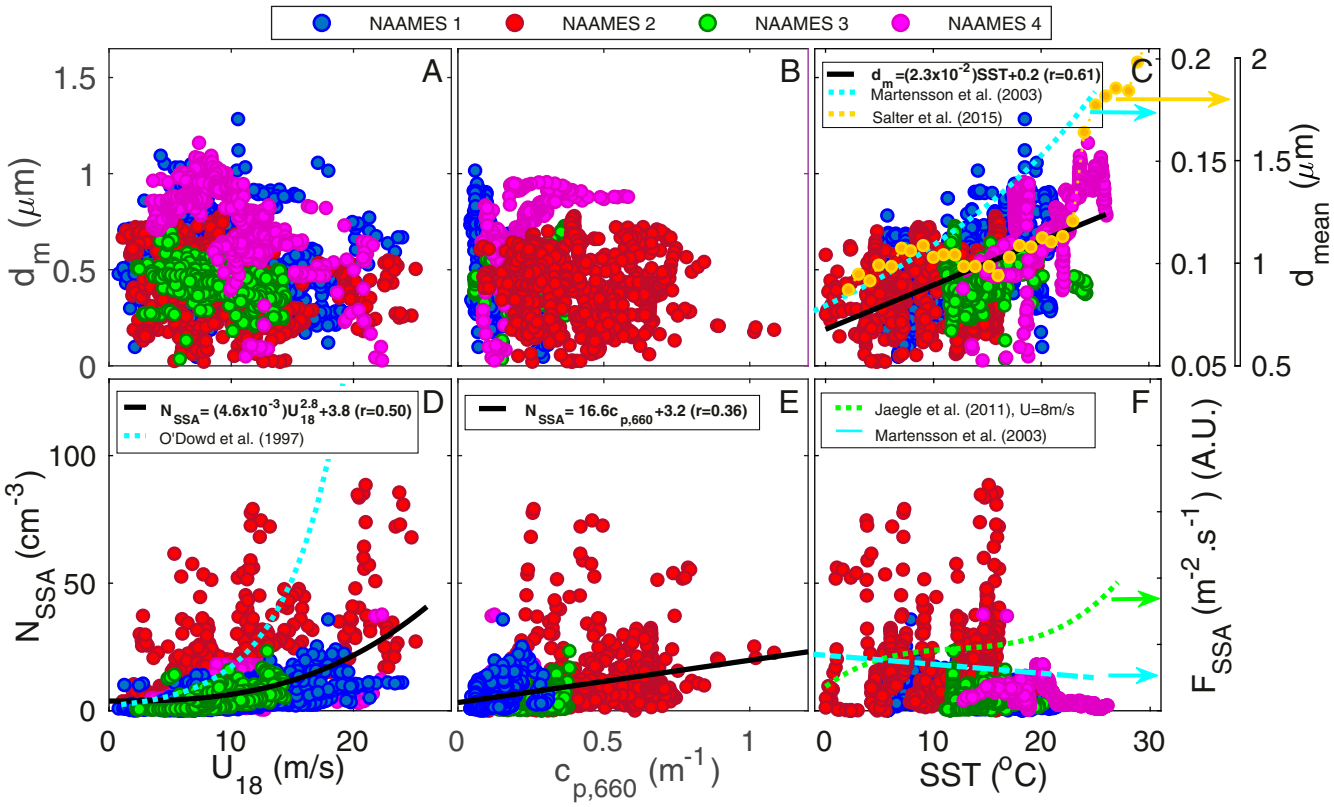

Fig. 3. SSA mode diameter (d_m) versus (*A*) wind speed (U_{18}), (*B*) seawater particle attenuation at 660 nm ($c_{p,660}$), (*C*) and SST. SSA number concentrations (N_{SSA}) versus (*D*) wind speed, (*E*) $c_{p,660}$, and (*F*) SST. The measurements are colored by campaign. Lines of best fit for all four NAAMES campaigns are plotted as solid black lines if $|R| > 0.3$. Published parameterizations are plotted as dotted colored lines. The dotted blue curve in *C* is the mean diameter of the flux size distribution from Mårtensson et al. (16) (first right *y* axis) and the dotted yellow curve in *C* is the mean diameter of the particle size distribution from Salter et al. (29) (second right *y* axis). The O'Dowd et al. (14) SSA parameterization versus wind speed is shown in (*D*) as a dotted blue line. SSA flux production versus SST from Jaeglé et al. (21) at a wind speed of 8 m s^{-1} (green dotted line right *y* axis) and SSA flux production from Mårtensson et al. (16) (blue dotted line, right *y* axis) versus SST are shown in *F*. Parameterization for d_m versus SST is shown in bold in *C*. The correlation between d_m and SST ($R = 0.61$) decreased when excluding NAAMES 4 measurements sampled at latitudes south of 30°N ($R = 0.46$).

is consistent with laboratory experiments (16, 20, 29, 31). For example, the mean diameter of the SSA distributions increased monotonically with SST, from 0.08 μm at SST = 0 °C to 0.18 μm at SST = 25 °C for Mårtensson et al. (16) and from 0.8 μm at SST = 2 °C to 2.0 μm at SST = 30 °C for Salter et al. (29) (Fig. 3*C*).

Implications for Climate Models. SST, local wind speed, and biomass measured during NAAMES explain some of the variability in SSA number concentrations and diameter. The retrieved SSA size distributions are broadly consistent with SSA parameterizations from O'Dowd et al. (14) and Lewis and Schwartz (1) (Fig. 4). However, the O'Dowd et al. (14) parameterization (based on measurements in the northeastern Atlantic) is clearly lower than the NAAMES N_{SSA} for particles with diameter larger than 0.5 μm, at all wind regimes and for all seasons. These larger SSA particles constitute more than 90% of retrieved SSA mass, which contributes the most to the direct aerosol radiative effects under open ocean conditions. For example, at low wind speeds, N_{SSA} was a factor of 2 larger for NAAMES 1, 3, and 4 than O'Dowd et al. (14) predictions and a factor of 5.0 larger for NAAMES 2 (climax biomass) for particles larger than 0.5 μm. Similarly, at high wind speeds, N_{SSA} was a factor of 1.5 larger for NAAMES 1, 3, and 4 than O'Dowd et al. (14) predictions and a factor of 9.2 larger for NAAMES 2. These results imply that global climate models with SSA production functions optimized to O'Dowd et al. (14) data may underestimate SSA concentrations for diameters larger than 0.5 μm (hence direct radiative effects), but may overestimate overall SSA concentrations (hence CCN) by a factor of 4 to 7 (*SI Appendix*, Fig. S8) for conditions where the single (broad) modes used here are sufficient to represent SSA. The limited evidence found for additional small particles for NAAMES 1 (*SI Appendix*, Text S5) could be relevant for SSA particle number concentrations (but likely not CCN), although additional investigation would be needed to attribute them quantitatively to SSA.

At low local wind speeds, NAAMES N_{SSA} were within 5 to 20% of N_{SSA} predicted by the Lewis and Schwartz (1) SSA parameterization for NAAMES 1, 3, and 4 (although the size and width of the SSA particle modes differ, Fig. 4), but a factor of 3 larger than predicted values during NAAMES 2 (late spring biomass climax). At high wind speeds, N_{SSA} predicted by Lewis and Schwartz (1) is higher than NAAMES N_{SSA} by a factor of 1.7 to 1.8 for NAAMES 1, 3, and 4, but smaller than NAAMES N_{SSA} by a factor of 1.7 for NAAMES 2.

If the O'Dowd et al. (14) SSA parameterization is used to calculate the scattering from SSA particles [using Mie theory (43); *SI Appendix*, Text S11], then the resultant scattering coefficient ($b_{sca\text{-}450}$) is lower than measured scattering during NAAMES by a factor of 2 to 5 on average (*SI Appendix*, Fig. S11). In addition, Mie-calculated $b_{sca\text{-}450}$ using the O'Dowd et al. (14) parameterization explains only 11 to 40% of the variability in measured $b_{sca\text{-}450}$ (*SI Appendix*, Fig. S12). These comparisons illustrate that the representation of SSA size distributions by the bimodal O'Dowd et al. (14) parameterization biases the scattering and consequently the direct radiative forcing of SSA (44).

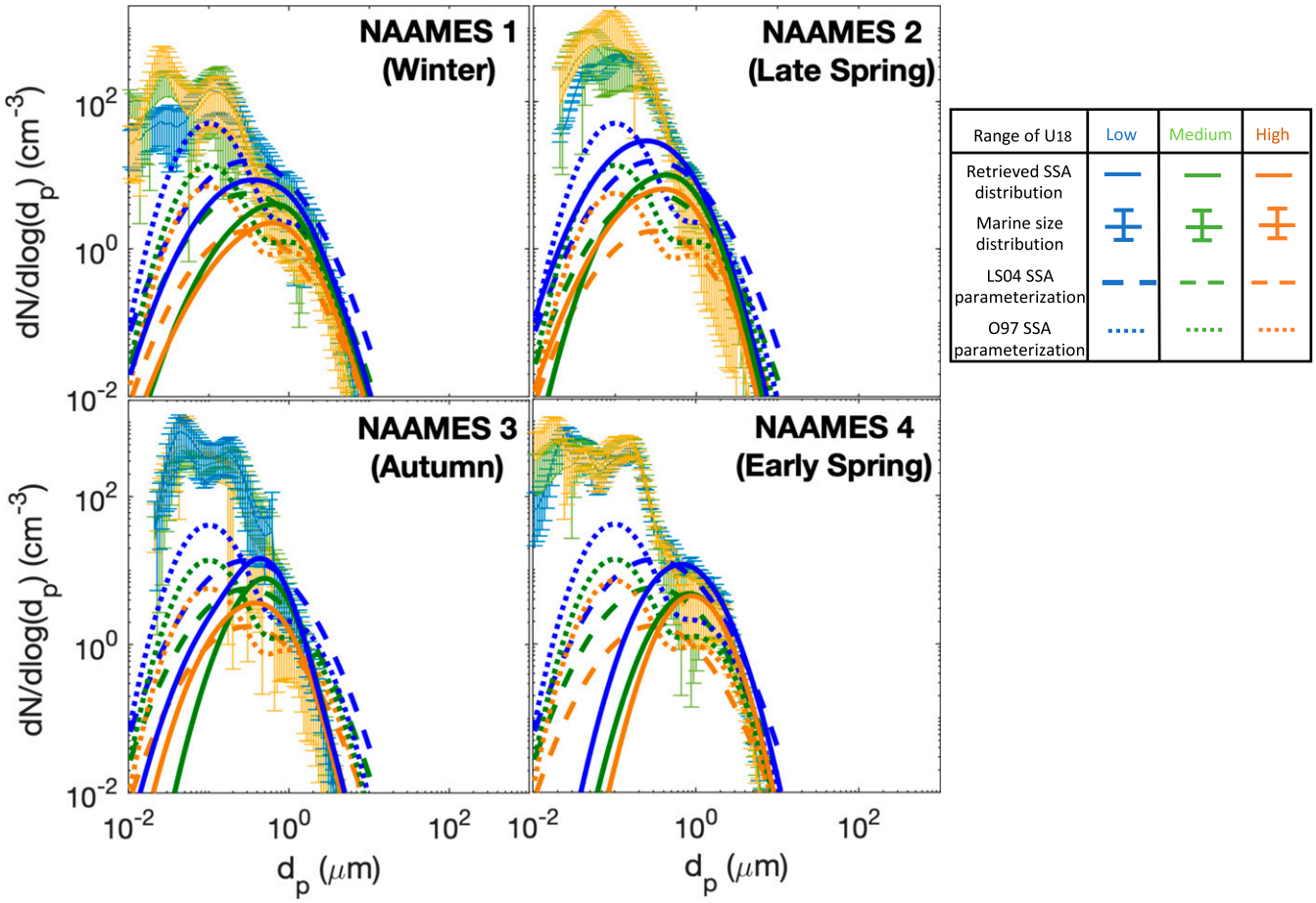

Fig. 4. Comparison of average retrieved SSA size distributions (solid colored lines) with SSA parameterizations from Lewis and Schwartz (1) (LS04, dashed colored lines) and O'Dowd et al. (14) (O97, dotted colored lines) for three wind regimes: low wind speeds (orange lines; 4.7 m s^{-1} < U_{18} < 5.3 m s^{-1} or 5.7 m s^{-1} < U_{18} < 6.3 m s^{-1} depending on available measurements), medium wind speeds (green lines; 8.7 m/s < U_{18} < 9.3 m/s), and high wind speeds (blue lines; 13.7 m s^{-1} < U_{18} < 14.3 m s^{-1} or 14.7 m s^{-1} < U_{18} < 15.3 m s^{-1} depending on available measurements). The average and SD for the measured marine size distributions, for each wind speed category, are given as the solid lines and error bars. The number of measurements is n = 17 (NA1), 50 (NA2),18 (NA3), and 17 (NA4) at low U_{18}; n = 31 (NA1), 31 (NA2), 36 (NA3), and 57 (NA4) at medium U_{18}; and n = 30 (NA1), 10 (NA2), 11 (NA3), and 17 (NA4) at high U_{18}.

Effects of SST and bacterial production on SSA and their scattering have begun to be incorporated in global climate model studies (29, 45–48). Our work shows that the single-mode SSA particle distributions retrieved from ambient measurements that maximize correlations to local wind speeds provide a factor of 4 to 7 fewer N_{SSA} (hence CCN) than parameterizations based on the O'Dowd et al. (14) bimodal SSA size distribution. Furthermore increases in SST lead to larger SSA mode diameters and not accounting for these increased particle sizes makes the direct radiative effects of SSA too low by a factor of 2 to 5 for the subarctic western Atlantic region measured here. The weak dependence on the $c_{p,660}$ biomass indicator could also explain some additional variability in sea spray number concentration, but the complexity of the ocean ecosystem drivers means that a simple linear dependence does not represent this relationship. Longer duration measurements of open-ocean seawater and aerosol properties would be needed to evaluate ecosystem-based models of the surface ocean.

Methods

NAAMES campaigns were conducted in winter 2015 (NAAMES 1), late spring 2016 (NAAMES 2), early autumn 2017 (NAAMES 3), and early spring 2018 (NAAMES 4) (latitudes > 40°N, except for NAAMES 4; *SI Appendix*, Table S2), with each campaign targeting a specific event in the annual phytoplankton biomass cycle (49). Shipboard aerosol measurements sampled isokinetically through an inlet (50), included aerosol number concentration, size distribution, chemical composition, and scattering coefficients. Additional shipboard measurements included wind speed and direction, relative humidity, SST, DOC, bacterial production rates, and $c_{p,660}$ (*SI Appendix*, Text S1).

Differential mobility measurements (TSI Differential Mobility Particle Sizer, or Brechtel Scanning Electrical Mobility Spectrometer based on availability) and TSI Aerodynamic Particle Sizer size distributions were merged (51) and then fitted for diameters larger than 0.6 μm to a single lognormal mode to obtain N_{SSA} and d_m (35, 36) for clean marine conditions (*SI Appendix*, Text S2). The extent to which d_m was driven by relative humidity (RH) was found to be small, with only 8% of the variability in retrieved d_m explained by ambient and sampling line RH (*SI Appendix*, Text S9). This approach included a comprehensive evaluation of clean marine conditions, densities used for merging, evaluation of the single lognormal mode, fitting algorithm and constraints, SE of fits and goodness of fits, and effects of relative humidity, as well as a comparison of retrieved SSA mass concentrations with ion chromatography Na^+ [obtained from filters collected on multijet cascade impactors (52)] and aerosol mass spectrometer measurements, and comparison with literature (*SI Appendix*, Text S2–S9 and S13).

The 15-min retrieved sea-spray aerosol number concentration, mode diameter, and geometric standard deviations are listed in a separate file as part of the *SI Appendix*. The fitting algorithm is shown in *SI Appendix, Text S14*.

ACKNOWLEDGMENTS. We thank the dedicated captain and crew of the Research Vessel *Atlantis* and the Marine Facilities at the Woods Hole Oceanographic Institution without whom the North Atlantic Aerosols and Marine Ecosystems Study (NAAMES) campaigns would have not been possible. We also would like to acknowledge Raghu Betha, Derek Price, Derek Coffman,

and Lucia Upchurch for collecting measurements. This work was funded by NASA grant NNX15AE66G and NSF OCE-1537943. This is PMEL contribution no. 4966. The views, opinion, and research findings contained in this paper are those of the authors and should not be construed as an official position of the funding agencies. This work is in compliance with the FAIR data principles.

1. E. R. Lewis, S. E. Schwartz, *Sea Salt Aerosol Production: Mechanisms, Methods, Measurements and Models—A Critical Review* (Geophysical Monograph Series, American Geophysical Union, Washington, DC, 2004).
2. P. K. Quinn, D. J. Coffman, V. N. Kapustin, T. S. Bates, D. S. Covert, Aerosol optical properties in the marine boundary layer during the first aerosol characterization experiment (ACE 1) and the underlying chemical and physical aerosol properties. *J. Geophys. Res.* **103**, 16547–16563 (1998).
3. D. M. Murphy *et al*., Influence of sea-salt on aerosol radiative properties in the Southern Ocean marine boundary layer. *Nature* **392**, 62–65 (1998).
4. P. K. Quinn *et al*., A comparison of aerosol chemical and optical properties from the 1st and 2nd Aerosol Characterization Experiments. *Tellus Ser. B Chem. Phys. Meteorol.* **52**, 239–257 (2000).
5. M. O. Andreae, D. Rosenfeld, Aerosol-cloud-precipitation interactions. Part 1. The nature and sources of cloud-active aerosols. *Earth Sci. Rev.* **89**, 13–41 (2008).
6. S. Twomey, The influence of pollution on the shortwave albedo of clouds. *J. Atmos. Sci.* **34**, 1149–1152 (1977).
7. T. J. Garrett, L. F. Radke, P. V. Hobbs, Aerosol effects on cloud emissivity and surface longwave heating in the Arctic. *J. Atmos. Sci.* **59**, 769–778 (2002).
8. N. Meskhidze *et al*., Production mechanisms, number concentration, size distribution, chemical composition, and optical properties of sea spray aerosols. *Atmos. Sci. Lett.* **14**, 207–213 (2013).
9. G. De Leeuw *et al*., Production flux of sea spray aerosol. *Rev. Geophys.* **49**, RG2001 (2011).
10. K. S. Carslaw *et al*., Large contribution of natural aerosols to uncertainty in indirect forcing. *Nature* **503**, 67–71 (2013).
11. H. Grythe, J. Ström, R. Krejci, P. Quinn, A. Stohl, A review of sea-spray aerosol source functions using a large global set of sea salt aerosol concentration measurements. *Atmos. Chem. Phys.* **14**, 1277–1297 (2014).
12. J. Ovadnevaite *et al*., On the effect of wind speed on submicron sea salt mass concentrations and source fluxes. *J. Geophys. Res.* **117**, D16201 (2012).
13. J. Kasparian *et al*., Assessing the dynamics of organic aerosols over the North Atlantic Ocean. *Sci. Rep.* **7**, 45476 (2017).
14. C. D. O'Dowd, M. H. Smith, I. E. Consterdine, J. A. Lowe, Marine aerosol, sea-salt, and the marine sulphur cycle: A short review. *Atmos. Environ.* **31**, 73–80 (1997).
15. P. Bikkina *et al*., Hydroxy fatty acids in remote marine aerosols over the Pacific Ocean: Impact of biological activity and wind speed. *ACS Earth Space Chem.* **3**, 366–379 (2019).
16. E. M. Mårtensson, E. D. Nilsson, G. de Leeuw, L. H. Cohen, H.-C. Hansson, Laboratory simulations and parameterization of the primary marine aerosol production. *J. Geophys. Res.* **108**, 4297 (2003).
17. E. C. Monahan, D. E. Spiel, K. L. Davidson, "A model of marine aerosol generation via whitecaps and wave disruption" in *Oceanic Whitecaps: And Their Role in Air-Sea Exchange Processes*, E. C. Monahan, G. M. Niocaill, Eds. (Springer, 1986) pp. 167–174.
18. S. L. Gong, A parameterization of sea-salt aerosol source function for sub- and super-micron particles. *Global Biogeochem. Cycles* **17**, 1097 (2003).
19. K. A. Prather *et al*., Bringing the ocean into the laboratory to probe the chemical complexity of sea spray aerosol. *Proc. Natl. Acad. Sci. U.S.A.* **110**, 7550–7555 (2013).
20. K. Sellegri, C. D. O'Dowd, Y. J. Yoon, S. G. Jennings, G. de Leeuw, Surfactants and submicron sea spray generation. *J. Geophys. Res.* **111**, D22215 (2006).
21. L. Jaeglé, P. K. Quinn, T. S. Bates, B. Alexander, J. T. Lin, Global distribution of sea salt aerosols: New constraints from in situ and remote sensing observations. *Atmos. Chem. Phys.* **11**, 3137–3157 (2011).
22. Y. Lehahn *et al*., Decoupling atmospheric and oceanic factors affecting aerosol loading over a cluster of mesoscale North Atlantic eddies. *Geophys. Res. Lett.* **11**, 3137–3157 (2014).
23. J. Zábori *et al*., Wintertime Arctic Ocean sea water properties and primary marine aerosol concentrations. *Atmos. Chem. Phys.* **12**, 10405–10421 (2012).
24. T. Dror, Y. Lehahn, O. Altaratz, I. Koren, Temporal-scale analysis of environmental controls on sea spray aerosol production over the South Pacific Gyre. *Geophys. Res. Lett.* **45**, 8637–8646 (2018).
25. E. Fuentes, H. Coe, D. Green, G. De Leeuw, G. McFiggans, On the impacts of phytoplankton-derived organic matter on the properties of the primary marine aerosol–Part 1: Source fluxes. *Atmos. Chem. Phys.* **10**, 9295–9317 (2010).
26. S. D. Forestieri *et al*., Temperature and composition dependence of sea spray aerosol production. *Geophys. Res. Lett.* **45**, 7218–7225 (2018).
27. L. M. Russell, L. N. Hawkins, A. A. Frossard, P. K. Quinn, T. S. Bates, Carbohydrate-like composition of submicron atmospheric particles and their production from ocean bubble bursting. *Proc. Natl. Acad. Sci. U.S.A.* **107**, 6652–6657 (2010).
28. J. Ovadnevaite *et al*., A sea spray aerosol flux parameterization encapsulating wave state. *Atmos. Chem. Phys.* **14**, 1837–1852 (2014).
29. M. E. Salter *et al*., An empirically derived inorganic sea spray source function incorporating sea surface temperature. *Atmos. Chem. Phys.* **15**, 11047–11066 (2015).
30. D. B. Collins *et al*., Direct aerosol chemical composition measurements to evaluate the physicochemical differences between controlled sea spray aerosol generation schemes. *Atmos. Meas. Tech.* **7**, 3667–3683 (2014).
31. R. L. Modini, L. M. Russell, G. B. Deane, M. D. Stokes, Effect of soluble surfactant on bubble persistence and bubble-produced aerosol particles. *J. Geophys. Res.* **118**, 1388–1400 (2013).
32. C. D. O'Dowd *et al*., Biogenically driven organic contribution to marine aerosol. *Nature* **431**, 676–680 (2004).
33. A. Engel *et al*., The ocean's vital skin: Toward an integrated understanding of the sea surface microlayer. *Front. Mar. Sci.* **4**, 165 (2017).
34. W. D. Gardner, A. V. Mishonov, M. J. Richardson, Global POC concentrations from in-situ and satellite data. *Deep Sea Res. Part II Top. Stud. Oceanogr.* **53**, 718–740 2006.
35. R. L. Modini *et al*., Primary marine aerosol-cloud interactions off the coast of California. *J. Geophys. Res.* **120**, 4282–4303 (2015).
36. P. K. Quinn, D. J. Coffman, J. E. Johnson, L. M. Upchurch, T. S. Bates, Small fraction of marine cloud condensation nuclei made up of sea spray aerosol. *Nat. Geosci.* **10**, 674–679 (2017).
37. A. D. Clarke, S. R. Owens, J. Zhou, An ultrafine sea-salt flux from breaking waves: Implications for cloud condensation nuclei in the remote marine atmosphere. *J. Geophys. Res. Atmos.***111**, D06202 (2006).
38. C. A. Carlson, D. A. Hansell, "DOM sources, sinks, reactivity, and budgets" in *Biogeochemistry of Marine Dissolved Organic Matter*, D. A. Hansell, C. A. Carlson, Eds. (Academic Press, ed. 2, 2015), pp. 65–126.
39. A. A. Frossard *et al*., Sources and composition of submicron organic mass in marine aerosol particles. *J. Geophys. Res. Atmos.* **119**, 12977–13003 (2014).
40. J. R. Pierce, P. J. Adams, Global evaluation of CCN formation by direct emission of sea salt and growth of ultrafine sea salt. *J. Geophys. Res. Atmos.* **111**, D06203 (2006).
41. I. R. Jenkinson, S. Laurent, H. Ding, F. Elias, Biological modification of mechanical properties of the sea surface microlayer, influencing waves, ripples, foam and air-sea fluxes. *Elem. Sci. Anth.* **6**, 26 (2018).
42. L. N. Hawkins, L. M. Russell, Polysaccharides, proteins, and phytoplankton fragments: Four chemically distinct types of marine primary organic aerosol classified by single particle spectromicroscopy. *Adv. Meteorol.* **2010**, 1–14. (2010).
43. C. F. Bohren, D. R. Huffman, *Absorption and scattering of light by small particles* (John Wiley & Sons, New York, NY, 1983).
44. P. K. Quinn, S. F. Marshall, T. S. Bates, D. S. Covert, V. N. Kapustin, Comparison of measured and calculated aerosol properties relevant to the direct radiative forcing of tropospheric sulfate aerosol on climate. *J. Geophys. Res.* **100**, 8977–8991 (1995).
45. S. M. Burrows *et al*., A physically based framework for modeling the organic fractionation of sea spray aerosol from bubble film Langmuir equilibria. *Atmos. Chem. Phys.* **14**, 13601–13629 (2014).
46. S. M. Burrows *et al*., OCEANFILMS-2: Representing coadsorption of saccharides in marine films and potential impacts on modeled marine aerosol chemistry. *Geophys. Res. Lett.* **43**, 8306–8313 (2016).
47. J. Golaz *et al*., The DOE E3SM coupled model version 1: Overview and evaluation at standard resolution. *J. Adv. Model. Earth Syst.* **11**, 2089–2129 (2019).
48. X. Liu *et al*., Toward a minimal representation of aerosols in climate models: Description and evaluation in the Community Atmosphere Model CAM5. *Geosci. Model Dev.* **5**, 709–739 (2012).
49. M. J. Behrenfeld *et al*., The North Atlantic Aerosol and Marine Ecosystem Study (NAAMES): Science motive and mission overview. *Front. Mar. Sci.* **6**, 122 (2019).
50. T. S. Bates, D. J. Coffman, D. S. Covert, P. K. Quinn, Regional marine boundary layer aerosol size distributions in the Indian, Atlantic, and Pacific Oceans: A comparison of INDOEX measurements with ACE-1, ACE-2, and Aerosols99. *J. Geophys. Res. Atmos.* **107**, INX2 25-1–INX2 25-15 (2002).
51. A. Khlystov, C. Stanier, S. N. Pandis, An algorithm for combining electrical mobility and aerodynamic size distributions data when measuring ambient aerosol. *Aerosol Sci. Technol.* **38**, 229–238 (2004).
52. A. Berner, C. Lürzer, F. Pohl, O. Preining, P. Wagner, The size distribution of the urban aerosol in Vienna. *Sci. Total Environ.* **13**, 245–261 (1979).